Chapter 11

CALIXARENES ON MOLECULAR PRINTBOARDS

Multivalent binding, capsule formation, and surface patterning

Manon J. W. Ludden, Mercedes Crego-Calama, David N. Reinhoudt, and Jurriaan Huskens

Laboratory of Supramolecular Chemistry and Technology, MESA+ Institute for Nanotechnology, University of Twente, P.O. Box 217, 7500 AE Enschede, The Netherlands

Abstract: The divalent binding of bis(adamantyl)-calix[4]arene **4** in solution and at β-cyclodextrin (β-CD) self-assembled monolayers (SAMs) (**2**) has been investigated. At β-CD SAMs the binding constant is three orders of magnitude higher than the binding constant for the divalent binding of **4** to the β-CD dimer **3** in solution (1.2×10^7 M^{-1}). A model that treats the sequential binding events as independent, and takes into account an effective concentration term for the second, intramolecular, binding event explains these results. The build-up and subsequent break-down of a non-covalent capsule consisting of tetra(adamantyl)-calix[4]arene **5** and tetrasulfonate-calix[4]arene **6** at the β-CD SAM was studied by surface plasmon resonance (SPR) spectroscopy. The association constant for capsule formation at β-CD SAMs ($(3.5 \pm 1.6) \times 10^6$ M^{-1}) is comparable to the association constant of the capsule in solution ($(7.5 \pm 1.2) \times 10^5$ M^{-1}). Microcontact printing (μCP) and dip-pen nanolithography (DPN) were applied in the patterning of β-CD SAMs. Stable features were obtained upon printing and writing of the bis(adamantyl)-calix[4]arene **4** at the β-CD SAMs. The features could not be removed upon rinsing with water, while rinsing with 10 mM β-CD resulted in partial removal of the patterns. In contrast features printed at OH-terminated SAMs were removed instantly upon rinsing with water.

Key words: Cyclodextrins; self-assembled monolayers; host-guest interactions; multivalency; non-covalent capsules; surface patterning; microcontact printing; dip-pen nanolithography.

J. Vicens and J. Harrowfield (eds.), Calixarenes in the Nanoworld, 213–231.

1. INTRODUCTION

The precise positioning of molecules at a surface is a prerequisite for the build-up of nanosized objects at surfaces. In our group, β-cyclodextrin (β-CD) self-assembled monolayers (SAMs)[1,2] are utilized as a template in this positioning process.[3,4] β–CD is a very well known host in aqueous media for a variety of small hydrophobic organic guest molecules, e.g. ferrocene, aromatic compounds, and adamantyl derivatives,[5] each with its own intrinsic binding affinity.[5] A β-CD SAM can therefore serve as a host surface for these molecules. A β-CD SAM consists of self-assembled β-CDs which are modified at the primary side with seven heptathioether chains.[1,2] On gold, the formed SAM is quasi-hexagonally, densely packed[1,2] and has a well-defined lattice constant (2.1 nm),[6] as determined by atomic force microscopy (AFM). All guest-binding sites in the β-CD SAM are equivalent. Since these host molecules are positioned in a very regular pattern, these surfaces are referred to as "molecular printboards".[3,7] According to surface plasmon resonance (SPR)[2,8] and electrochemical impedance spectroscopy (EIS) measurements,[2] the binding constants (K) of small monovalent molecules at the molecular printboard are comparable to the binding constants of these molecules to native β-CD in solution.[6]

Multivalent interactions are widespread in nature and supramolecular chemistry and describe the simultaneous binding of multiple guest entities on one molecule to multiple host entities on another.[9] Multivalent binding processes differ markedly from monovalent binding processes, e.g. they consist of inter- and intramolecular interactions, and dissociation is in general slow and can be influenced by a competitor in solution.[9]

An example of a multivalent system is that of a tris(vancomycin) derivative and a tris(di-peptide) (D-alanine-D-alanine).[10,11] This system has a very high binding constant ($K_a = (4 \pm 1) \times 10^{17}\ M^{-1}$) even higher than that of the binding between (strept)avidin and biotin, which is regarded to be one of the strongest interactions in nature. The dissociation mechanism of the trivalent vancomycin system involves a sequence of successive dissociation events at the vancomycin binding sites, the rate of which can be influenced by a monovalent competitor in solution. Another example is the interaction between the heat-labile enterotoxin from E. Coli and some pentavalent ligands.[12] These pentavalent ligands are excellent inhibitors for the enterotoxin, while the lower valent ligands do not show the same level of inhibition. Also at surfaces multivalent binding processes have been studied, e.g. the aggregation of membrane-bound synthetic receptors[13] and the binding of multivalent ligands at cell surfaces.[14] These studies, however, do not provide many quantitative details, mainly because models that describe multivalent binding at surfaces are still under development.[15]

Multivalent interactions are not only important in nature, but they are also crucial when one wants to develop stable assemblies at surfaces. Multivalent host-guest interactions allow for controllable adsorption and desorption by variation of the type and number of host-guest interactions.[3] By making use of host-guest interactions, it may become possible to build nanosized structures such as capsules in a controlled fashion on a molecular printboard. The same interactions can also be exploited for creating patterns of molecules on surfaces through supramolecular microcontact printing (μCP) or dip-pen nanolithography (DPN).

In this chapter we describe a model which allows the quantitative understanding of multivalent interactions at surfaces.[15,16] In this model, a β-CD SAM serves as a host surface, and a bis(adamantyl)-functionalized calix[4]arene serves as a multivalent guest. Furthermore, applications are shown that require kinetically and/or thermodynamically stable interactions. We show that it is possible to build a non-covalent capsule on a β-CD SAM making use of orthogonal host-guest and ionic interactions,[17] and that it is possible to pattern β-SAMs by microcontact printing (μCP) and dip-pen nanolithography (DPN).[7]

2. MULTIVALENT CYCLODEXTRIN HOST-GUEST INTERACTIONS IN SOLUTION AND AT THE MOLECULAR PRINTBOARD

Multivalent binding assuming independent binding sites, i.e. without cooperativity, can be described quantitatively in several ways. One is to analyze multivalent binding based on intrinsic binding constants and effective concentrations.[12,18,19] The intrinsic binding constant (K_i) describes the interaction of the monovalent recognition motif, while the effective concentration is used to differentiate between inter- and intramolecular binding steps, and represents the probability of interaction between two complementary interacting sites in an intramolecular binding event. Effective concentration[18-21] is conceptually similar to effective molarity,[20,22] which represents the ratio of association constants for intra- and intermolecular processes. The effective concentration symbolizes a "physically real" concentration of one of the interacting sites as experienced by its complementary counterpart in the probing volume determined by the covalent or non-covalent linker between them. The effective concentration is thus dependent on the linker length and the structure of the molecules. Such a model was used by Lees et al.[12] to describe the binding of multivalent inhibitors for Shiga-like toxins. Another way to describe multivalency is in entropy terms as proposed by Whitesides and coworkers.[9,11] When dealing

with independent binding sites, the overall binding enthalpy is the sum of the binding enthalpies of the individual interactions. Although the basic assumptions of both treatments are the same, the correct interpretation of the entropy terms in multivalent binding is not trivial. Therefore, the approach based on intrinsic binding constants and effective concentration will be used here, because stability constants of the interactions between guest and host molecules in solution as well as at the molecular printboard can be easily obtained.

As a model system to understand multivalent binding at interfaces in a quantitative sense, we have compared the binding of calix[4]arene **4** to β-CD (**1**) and a β-CD dimer **3** in solution and to the β-CD printboard **2** (see Fig. 1).[16]

Thermodynamic data on the binding of **4** in solution were obtained from isothermal titration calorimetry (ITC). Figure 2 shows enthalpograms obtained for the binding of **4** to native β-CD (**1**) (Fig. 2a) and to the β -CD dimer **3** (Fig. 2b). When β-CD was titrated to **4**, the inflection point of the curve occurred at a [β-CD]/[**4**] ratio of 2, which indicates a 2:1 host-guest binding mode, *i.e.* two β-CDs are bound to **4**. The ITC curve was fitted to a model in which independent binding sites are assumed, and in which the intrinsic association constant, K_i, and the binding enthalpy, ΔH_i, of the monovalent interaction were used as independent fitting parameters. The intrinsic binding constant (4.6×10^4 M^{-1}) and the binding enthalpy (-7.0 kcal/mol) obtained after fitting are typical for a β-CD-adamantyl interaction (see Table 1). The quality of the fit indicates that the binding mode is indeed 2:1, and that the assumption of independent binding sites is valid.

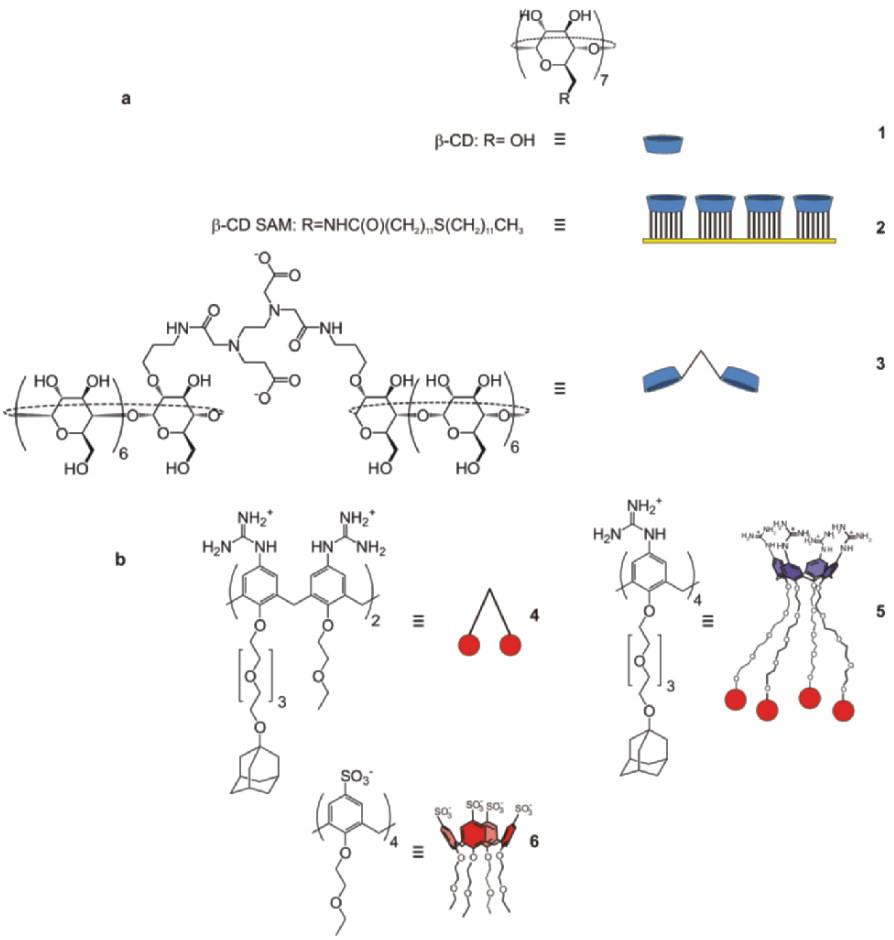

Figure 11-1. a) Host molecules: β-CD (1), the β-CD SAM **2**, and an EDTA-linked β-CD dimer **3**. b) Guest molecules employed here: a bis(adamantyl)-calix[4]arene **4**, a tetra-(adamantyl)-calix[4]arene **5**, and a tetrasulfonate-calix[4]arene **6**.

The enthalpogram of the titration of the divalent guest **4** to the β-CD dimer **3** is depicted in Fig. 2b. The inflection point in this case occurred at a [**4**]/[**3**] ratio of 1, indicating a 1:1 binding mode. The curve was fitted to a 1:1 binding model, using the overall binding enthalpy and association constant as independent fitting parameters. The fit gave thermodynamic parameters that are typical of a divalent interaction, the binding constant (1.2×10^7 M^{-1}) is more than two orders of magnitude higher than the intrinsic binding constant for a single adamantyl- β-CD interaction, while the binding enthalpy (–14.8 kcal/mol), within experimental error, is exactly twice as high as the value for the intrinsic binding enthalpy of **4** to one β-CD molecule. The latter is a clear indication that the two adamantyl moieties of **4** also behave as independent binding sites in the binding to the divalent host **3**. The main question regarding a quantitative understanding of multivalency relates thus to a mathematical relationship between the stability constants of the monovalent and multivalent systems.

Table 11-1. Thermodynamic parameters of the complexation of **4** to **1** (β-CD) and **3** (β-CD dimer), as determined by ITC.

host	Stoichiometry (host : guest)	K (M^{-1})	$\Delta G°$ (kcal/mol)	$\Delta H°$ (kcal/mol)	$T\Delta S°$ (kcal/mol)
1	2 : 1	$(4.6 \pm 0.3) \times 10^4$	–6.4 ± 0.1	–7.0 ± 0.5	–0.6 ± 0.6
3	1 : 1	$(1.2 \pm 0.3) \times 10^7$	–9.6 ± 0.1	–14.8 ± 0.5	–5.1 ± 0.6

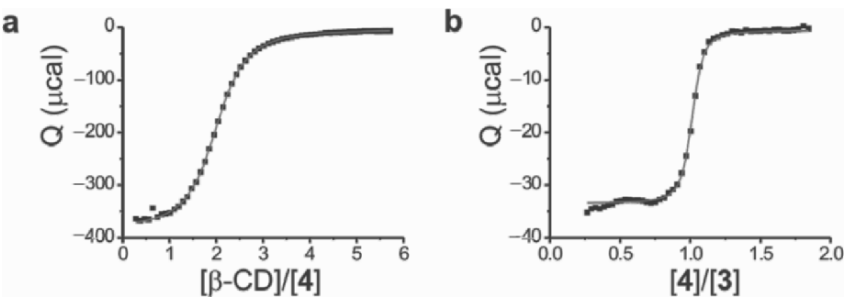

Figure 11-2. Heat evolved per injection plotted against the molar ratio (markers) and fits (solid lines) to 2:1 and 1:1 models, respectively, for the isothermal microcalorimetric titrations (25 °C) of **1** (10 mM) to **4** (0.4 mM) and of **4** (0.4 mM) to **3** (0.05 mM) in water.

Figure 3a schematically depicts the stepwise binding process of **4** to **3**. The first, intermolecular, interaction (K_1) is directly related to the intrinsic binding constant ($K_{i,l}$): $K_1 = 4K_{i,l}$, where the coefficient 4 is statistical. The subsequent intramolecular association step is the product of the intrinsic association rate constant and an effective concentration term, C_{eff}, which

reflects the concentration of uncomplexed host (β-CD) that is experienced by the uncomplexed adamantyl moiety that is linked to this free host site via a non-covalent linker incorporating the host-guest pair formed in the first step. Since the second dissociation step is twice as likely as the intrinsic dissociation, the equilibrium constant of the second step is given by: $K_2 = ½K_{i,l}C_{eff}$.

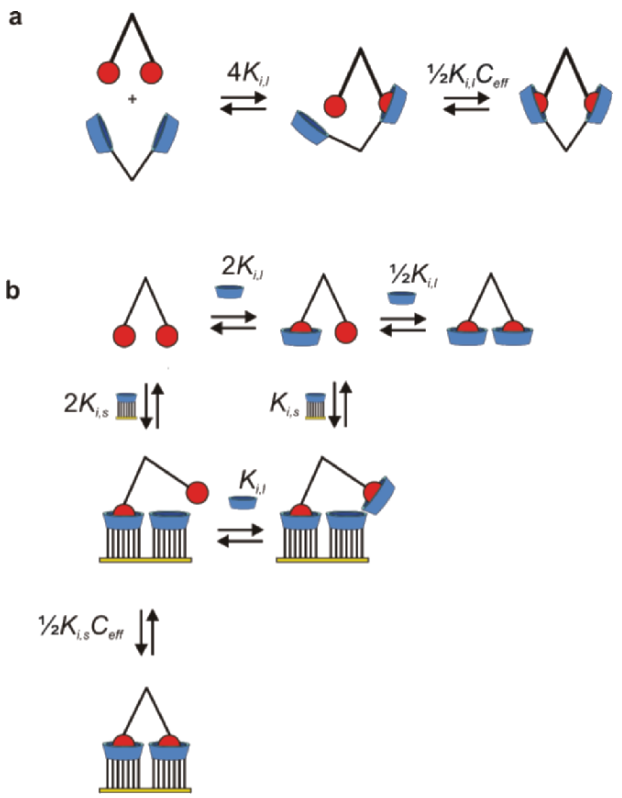

Figure 11-3. Equilibria for the sequential binding of **4** to **3** (a) and for the sequential binding of **4** to the molecular printboard in the presence of competing β-CD in solution (b).

Thus, assuming independent binding sites for the divalent interaction between **4** and **3**, the overall binding process can be described according to Eq. (1):

$$K = K_1 K_2 = 2K_i^2 C_{eff} \qquad (1)$$

As described above, the empirical effective molarity, EM, here given by $EM = ½K/K_i^2$ (Eq. 1), can now be calculated to be 2.8 ± 0.6 mM.

The effective concentration can be estimated theoretically using the formula for cyclization probability.[21,23] It can be conveniently approximated by Eq. 2:

$$C_{eff} = \frac{3}{4\pi < r_0 >^3 N_{AV}} \qquad (2)$$

Here, N_{AV} is Avogadro's constant, and $<r_0>$ is the radius of the probing volume (Fig. 4a). Eq. (2), shows that C_{eff} has an inverse cubic relation to $<r_0>$ Furthermore, this approximation allows extension to multivalent binding at the molecular printboard (see below; Figure 9.4b). The radius of the probing volume is in this case defined by the average end-to-end distance between the complexed and uncomplexed guest moieties.[19,20]

An estimate for the average root-mean-square end-to-end distance, $<r_0>$, can be obtained using three-dimensional random walk statistics,[23] which gave values for C_{eff} ranging from 1.8 to 92 mM, depending on which chain stiffness is assumed. The experimentally determined *EM* of 2.8 mM is within this range of calculated theoretical C_{eff} values. The relatively low value for the experimentally determined *EM* implies that the rotational mobility of the linker within the monovalent complex of **4** and **3** (Fig. 4a) is limited.

The binding of **4** to the molecular printboard was studied by SPR spectroscopy. Figure 5 shows five titration curves obtained from SPR titration experiments at different backgrounds of β-CD in solution. The experiments consisted of the addition of an increasing amount of a 1 μM solution of **4** to the molecular printboard at a constant β-CD concentration in solution. The addition of **4** resulted in each case in a change of the SPR angle, which indicated adsorption of **4** to the surface. In strong contrast, similar experiments performed on an 11-mercapto-1-undecanol SAM did not show adsorption. These SAMs are also OH-terminated like the molecular printboards, but lack the β-CD cavities and thus serve as reference layers.

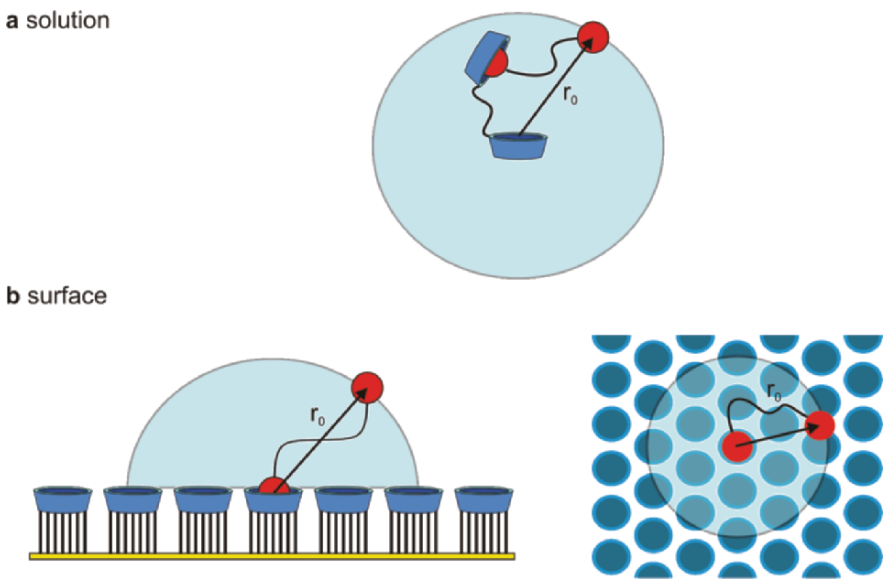

Figure 11-4. Schematic representation of the concept of effective concentration for the interactions between **4** and **3** (a) and of **4** to the molecular printboard (b).

After every addition, repeated rinsing with a competing solution, i.e. containing a high concentration of β-CD, resulted in desorption of **4** from the surface. The binding curve at 0.1 mM β-CD showed near-quantitative binding of **4** to the molecular printboard, prohibiting accurate determination of the binding constant. Reliable binding constants could only be obtained when using β-CD concentrations higher than 0.1 mM, to induce competition between binding of **4** to the molecular printboards vs. binding to β-CD in solution. From fitting the curves of Figure 5 to Langmuir isotherms, all complexation constants were about 10^{10} M^{-1}. This means that the binding constant at the surface is two to three orders of magnitude higher than the binding constant of **4** to **3** in solution.

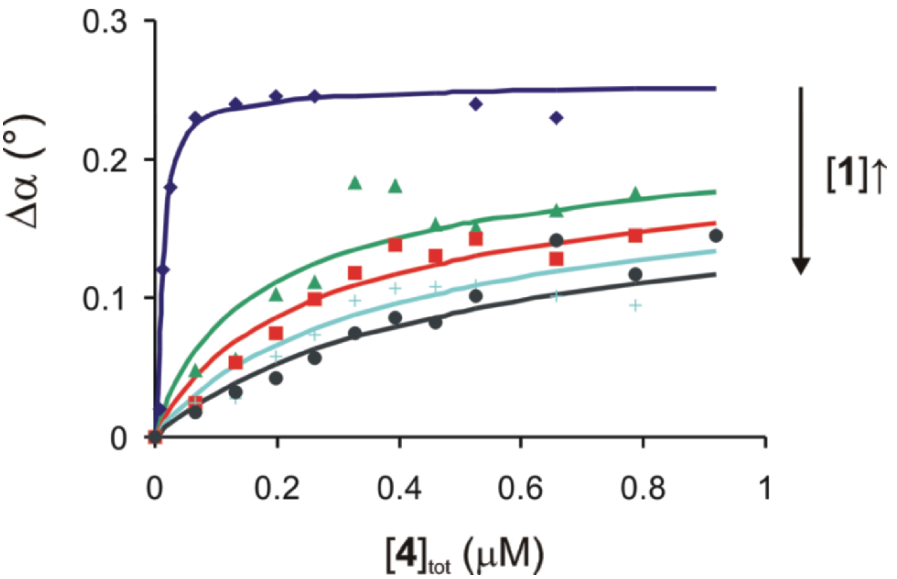

Figure 11-5. SPR angle data (markers) and corresponding fits to the sequential binding model (solid lines) for titrations of **4** to the molecular printboard at five different β-CD (**1**) background concentrations (♦ = 0.1 mM; ▲ = 0.5 mM; ■ = 1 mM; + = 2.5 mM; ● = 5 mM). Errors on the data points are approx. 0.02°. Arrows indicate a decrease of the slope upon an increasing concentration of β-CD (**1**).

This difference in binding affinities between solution and surface can be explained by the higher effective concentration at the surface. Again, the binding process is described by two sequential, independent binding events, which can take place in solution and/or at the surface (Fig. 3b). The solution species that are present are shown in the top row; from top to bottom, the equilibria for binding to the surface are shown. The binding events at the surface are considered to be equal and independent, just as in solution. This means that all binding events can be expressed in terms of intrinsic binding constants. The intrinsic binding constants in solution and at the surface are defined as $K_{i,l}$ (shown above to be 4.6 x 10^4 M^{-1}) and $K_{i,s}$, respectively.

The only intramolecular binding event at the surface, the formation of the bottom species in Fig. 3b, is again associated with an effective concentration term, similar to the second binding event for the sequential divalent binding of **4** in solution. Within this probing volume, several host molecules can be found to which the uncomplexed guest moiety may bind in an intramolecular fashion. Depending on the surface coverage, Θ, of the immobilized host cavities, however, not all hosts may be accessible.

The methodology used for the approximation of the maximal effective concentration $C_{eff,\max}$ *i.e.* the C_{eff} at low coverage, at the molecular printboard is similar to that used for the approximation of C_{eff} in solution. The difference is that at the surface the number of accessible host molecules is larger than 1, and that the linker length, $<r_0>$ results from the guest only, leading to a smaller probing volume. If the effective concentration concept is applied to the molecular printboard, Eq. 3 is obtained, in which A_{CD} is the surface area covered by a single β-CD host on the molecular printboard.

$$C_{eff} = \frac{3}{2A_{CD}N_{AV} < r_0 >}(1-\Theta) \tag{3}$$

In this case, $C_{eff,max}$ scales with $<r_0>^{-1}$ and therefore, the effective concentration at the surface is less dependent on $<r_0>$ than in solution (in solution C_{eff} scales with $<r_0>^{-3}$ see above). Consequently, the approximation of $C_{eff,max}$, (*i.e.* C_{eff} at Θ = 0) based on a range of $<r_0>$ values, gives a relatively narrow range of $C_{eff,max}$ values. Analogous to the solution case, the lower limit of $C_{eff,max}$ of 0.20 M was chosen for fitting of the SPR titration curves.

The SPR curves were fitted to this model using a least-squares optimization routine and treating $K_{i,s}$ and $\Delta\alpha_{max}$ as variables, while using fixed values for $K_{i,l}$ and $C_{eff,max}$. The fitting of the SPR curves of Fig. 5 using this multivalency model gave $K_{i,s}$ values at different β-CD background concentrations of approx. 3×10^5 M^{-1}. This value is comparable to the K_i value of small monovalent adamantyl guest molecules at the molecular printboard. Thus the assumption of independent binding sites at the interface also holds for the divalent binding of **4**. Furthermore, it clearly shows that the multivalency model provides a deeper insight into the true nature of the observed binding enhancements, both relative to monovalent binding and relative to divalent binding in solution. The high effective concentration at the interface is the main cause for these binding enhancements, and no cooperativity needs to be assumed to explain the experimental observations.

3. CAPSULE FORMATION AT THE MOLECULAR PRINTBOARD

Multivalent interactions can provide such high binding constants that molecules can be positioned on molecular printboards in a both thermodynamically and kinetically stable fashion. This phenomenon can be applied in the localized assembly formation leading to patterns of host-guest complexes (see section 4 below) and in the formation of more complicated

non-covalent structures at interfaces. Regarding the latter, we chose to build an ionic capsule at the printboard based on host-guest interactions.[17]

Much research has already been performed on the formation of non-covalent capsules in solution, *e.g.* for the encapsulation of drugs and the active transport or delivery of these drugs,[24] or for catalysis.[25] There are, however, only few cases in which capsules are self-assembled at a surface.[26-28] In those cases, the bottom part of the capsule was connected directly at the solid substrate via self-assembly of thiols on gold. Here we use orthogonal host-guest and ionic interactions to allow a stepwise build-up and break-down of the capsules at the molecular printboards (Fig. 6).

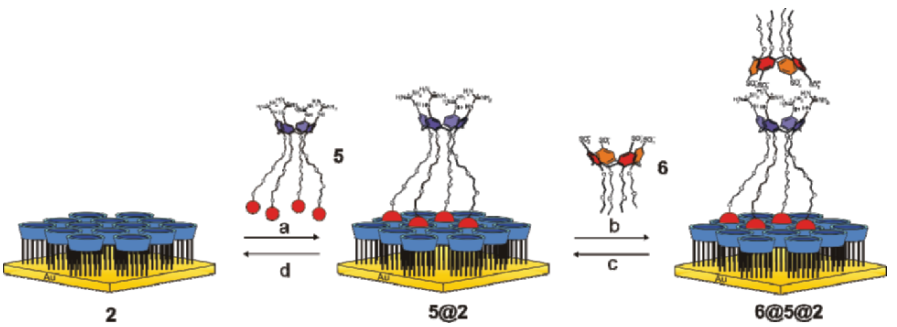

Figure 11-6. Schematic representation of the build-up (a,b) and subsequent break-down (c,d) of the capsule **6@5** at the molecular printboard.

The capsule consists of calix[4]arenes **5** and **6** (Fig. 1). The bottom part of the capsule is calix[4]arene **5**, the lower rim of which is modified with four oligo(ethyleneglycol) chains which each possess an adamantyl functionality, while the upper rim is modified with four guanidinium groups to increase water solubility. The top part of the capsule is the tetrasulfonate calix[4]arene **6**. The resulting capsule is based on the ionic interactions between the two oppositely charged upper rims of these calix[4]arenes.

ITC studies, in the presence of 10 mM β-CD to complex all adamantyl groups of **5**, showed that capsule formation in solution is an endothermic, entropy-driven process, with an association constant $K = (7.5 \pm 1.2) \times 10^5$ M^{-1}. The driving force for the capsule formation is the desolvation of the charged groups upon complex formation. The ITC enthalpogram indicates a 1:1 complex stoichiometry. Also, NMR experiments showed the formation of a well defined assembly.

For studying the surface assembly, the binding of **5** to the molecular printboard was studied first. In an SPR measurement, **5** was adsorbed at the molecular printboard at a β-CD background of 4 mM. The absolute increase of the signal, ~0.2° is very close to the absolute increase of the SPR signal

when **4** was adsorbed, which indicates a surface coverage of **5** comparable to **4**. In contrast to the binding of the divalent **4** however, the binding of **5** to the molecular printboard proved to be irreversible, as it appeared impossible to remove **5** by extensive rinsing procedures in which competition was induced by using a high concentration of native β-CD in solution (8 mM). Similarly, rinsing with 1 M KCl did not result in the removal of **5**. This is explained by the multivalency model described in section 2; the association constant of **5** to **2** is expected to be in the order of ~10^{15} M^{-1}. In contrast, subsequent rinsing procedures with methanol, ethanol and 2-propanol did result in the removal of **5** from the surface, by weakening the intrinsic hydrophobic interactions between the β-CD cavities and the adamantyl functionalities. Thus we have shown that the lower halve of the capsule can be strongly immobilized at the molecular printboard in aqueous solutions, but that the application of organic solvents provides a way of removing it from the surface again by lowering of $K_{i,s}$ and thus the stability of the assembly as a whole.

SPR titrations of the addition of **6** to a monolayer of **5** on the molecular printboard were performed, and fitted to a Langmuir isotherm. The association constant was $(3.5 \pm 1.6) \times 10^6$ M^{-1}, which is slightly higher than the association constant found in solution (7.5×10^5 M^{-1}). This could be due to some form of positive cooperativity, resulting from stronger electrostatic interactions of the many calixarenes **5** at the surface. However, the slightly higher association constant found on the surface compared to solution cannot be due to the formation of a 1:2 complex, because in that case an 8+/4- ion pair is to be expected, which should give rise to an association constant of approx. 10^{12} M^{-1}. It is obvious that the association constant observed here is far lower than this value.

The capsule could be built up in two steps at the molecular printboard, and broken down again in two steps (Fig. 6: a→b→c→d). This assembly and disassembly process can clearly be followed by SPR spectroscopy (Fig. 7). First a monolayer of **5** was formed at the molecular printboard (Figs. 6 and 7, step a). Subsequently, **6** was attached through ionic interactions on top of the monolayer of **5** (step b). At this point, the capsule is present at the molecular printboard. The stepwise assembly of the capsule is followed by the stepwise disassembly of the capsule. First, a rinsing procedure with 1 M KCl was performed (step c), in which the top part of the capsule, **6**, was removed by weakening of the ionic interactions due to charge screening at this high salt concentration. As noted before, this rinsing step does not affect the binding of **5** at the molecular printboard. After restoring the 10^{-2} M KCl background solution, a rinsing procedure with 2-propanol was applied in order to remove the bottom part of the capsule (step d). Hereafter the

molecular printboard appeared to be clean, since the whole procedure could be repeated without loss of efficiency (Fig. 7).

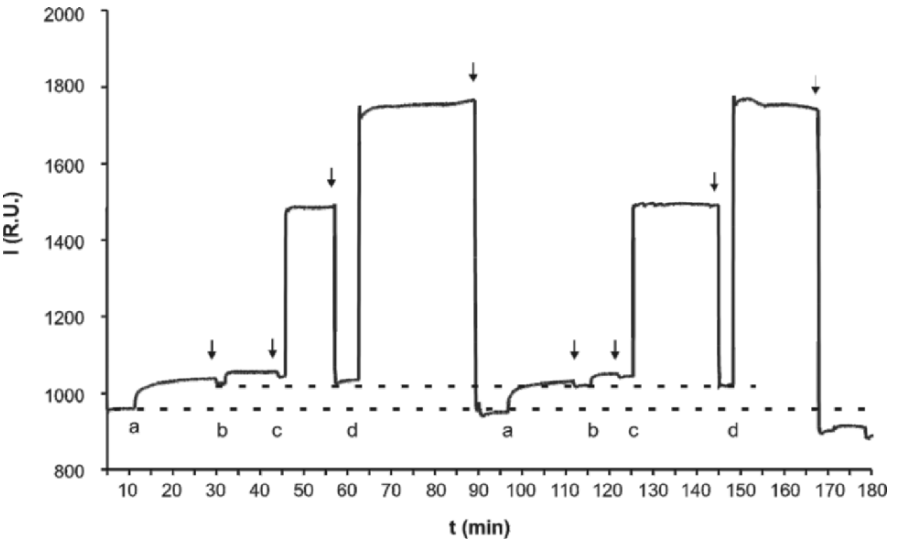

Figure 11-7. SPR sensogram showing the stepwise assembly and the subsequent stepwise disassembly of the molecular capsule **5@6** at the molecular printboard. The arrows (↓) indicate a background change to 10 mM aqueous KCl; *a* indicates adsorption of **5** (0.1 mM in 4.0 mM β-CD + 10 mM KCl); *b* indicates adsorption of **6** (0.1 mM in 4.0 mM β-CD + 10 mM KCl); *c* indicates desorption of **6** by 1 M KCl and *d* indicates desorption of **5** by 2-propanol.

In conclusion, these results show that multivalency can result in such strong binding that weaker, orthogonal interactions can be employed in subsequent steps to make more complex assemblies. Furthermore, it emphasizes the versatility of the molecular printboards as a building platform onto which assemblies can be constructed and removed again at will.

4. CREATING PATTERNS OF ASSEMBLIES AT THE MOLECULAR PRINTBOARD

As discussed above, thermodynamically and kinetically stable assemblies at molecular printboards can be created using the concept of multivalency. This bears the implication that also individual molecules or small groups can be firmly immobilized at predetermined positions. In this section, we discuss the creation of patterns based on supramolecular interactions at the molecular printboard using microcontact printing (μCP) and dip-pen nanolithography (DPN).[7]

μCP is parallel technique, developed by Whitesides *et al.* for the replication of relatively small patterns on surfaces, which is cost effective and fast.[29] Patterns are created by the transfer of molecules at the contact areas of a polymeric relief stamp with the substrate. Often poly(dimethyl siloxane) (PDMS) is used as a stamp material. In DPN, which is a serial technique, an AFM tip is inked, and the ink is transferred upon contact of the tip with the surface.[30,31] The patterns that are written can have a high resolution, and the transport of ink is controlled by a water meniscus between the tip and the sample.

Both techniques were applied for local transfer of **4** to the molecular printboard **2**. μCP of **4** yielded a pattern that was visible directly after printing (Fig. 8a), and remained visible after extensive rinsing with water (Fig. 8b). These results confirm the SPR studies described in section 2. Also extensive rinsing with 10 mM β-CD in solution did not completely remove the pattern, but led to loss of contrast due to partial removal of **4** induced by competition (Fig. 8c). The presence of **4** at the patterned areas of the substrate was also confirmed by secondary ion mass spectrometry (SIMS) (Fig. 8f). Analogously, **4** was printed onto a 11-mercapto-1-undecanol SAM. As can be seen in Figure 9.8d, **4** is transferred upon printing, but rinsing with water (Fig. 8e) was sufficient to remove **4** from the surface, attributable to the lack of host-guest interactions in this case.

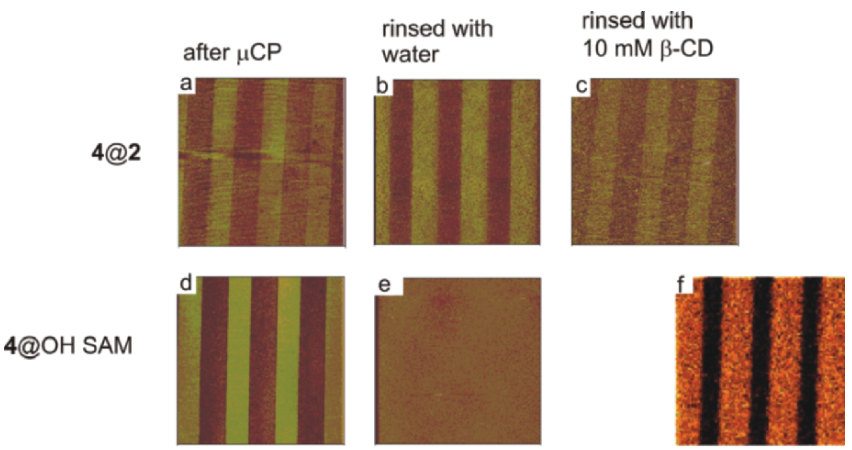

Figure 11-8. AFM friction force image (a-e; image size: 50 x 50 μm²) of patterns obtained by μCP of **4** (brighter areas) on the molecular printboard (a-c) and on OH-terminated SAMs (d,e) before rinsing (a,d), after rinsing with water (b,e), or after rinsing with 10 mM aqueous β-CD (e), respectively. TOF-SIMS image (f; image size: 56 x 56 μm²) of a β-CD SAM after μCP of **4**: the bright areas indicate the presence of the molecular ion peak of **4** at *m/z* = 1418.

In order to perform DPN nanolithography, silicon nitride AFM tips were dipped in aqueous solutions of **4**, and subsequently scanned across the molecular printboard, as well as on the OH-terminated reference SAMs. In both cases patterns were transferred (Figs. 9a and 9c). However, after rinsing with aqueous solutions, patterns were only visible at the molecular printboard, again indicating the need of multivalent host-guest interactions for pattern stability. To confirm that these patterns are not due to the mechanical force that was applied by the AFM tip to the surface, a reference experiment was performed in which a bare silicon nitride tip was used to write on the molecular printboard under the same conditions. These experiments did not show a visible pattern. The resolution that can be obtained by this method is below 100 nm, as shown by the line patterns in Fig. 9e. The line width is also in this case a function of contact time, tip radius, ink concentration, and ink-transfer mechanism.

Supramolecular multivalent interactions between the molecular printboard and a divalent guest can thus be employed in the patterning of surfaces. Stable, reversible, features are obtained upon printing and writing. The advantage of the use of supramolecular, multivalent interactions is the tunability and the reversibility of the system.

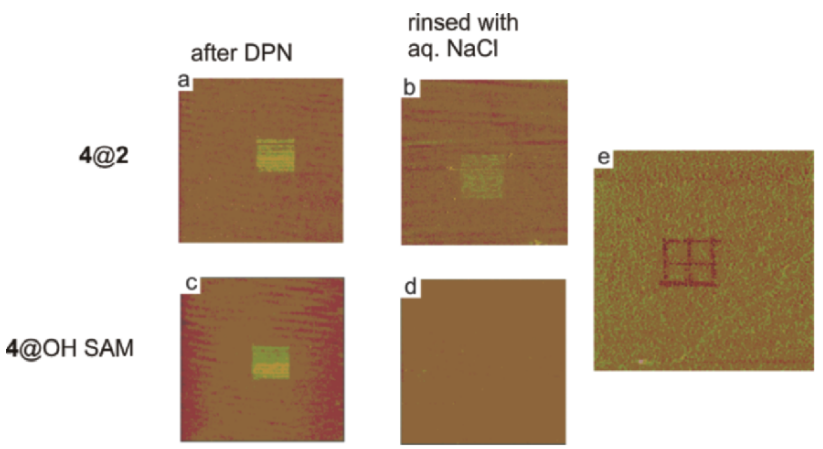

Figure 11-9. AFM friction force images (a-d; image size: 30 x 30 μm^2) showing patterns produced by DPN on the molecular printboard (a, b) and on OH-terminated SAMs (c, d) using **4** as the ink before rinsing (a, c), after rinsing in situ with with 50 mM aqueous NaCl (b, d), respectively. AFM friction force image (e; 4 x 4 μm^2; in air) showing an array of lines with mean widths of 60 ± 20 nm, produced by DPN of **4** at the molecular printboard.

5. CONCLUSIONS

Calix[4]arenes are versatile building blocks because of the possibility to modify the lower rim with multiple guest moieties in order to obtain multivalent systems. In section 2, a model is shown that describes multivalent binding processes in solution and at the surface. The binding of the bis(adamantyl)-calix[4]arene **4** to the molecular printboard has a binding affinity that is two to three orders of magnitude higher than the binding affinity for the divalent interaction between **4** and β-CD dimer **3** in solution. The model shows that this binding enhancement is due to a higher effective concentration at the surface.

Multivalent host-guest interactions can be employed to build larger non-covalent structures at surfaces. It was shown in section 3 that orthogonal interactions can be employed to create capsules at a surface. The bottom half of the capsule is a calix[4]arene modified at the lower rim with four guest moieties and at the upper rim with four guanidinium groups. This calix[4]arene is very strongly bound at the surface through four adamantyl-β-CD interactions. The top part of the capsule is a calix[4]arene modified at the upper rim with four sulfonate groups to enable capsule formation via ionic interactions with the guanidinium groups of the bottom half of the capsule. This capsule can be built up and broken down in subsequent steps at the molecular printboard.

Furthermore, it was shown in section 4 that supramolecular μCP and DPN can be used to create patterns based on multivalent host-guest interactions at a surface. These experiments showed that stable supramolecular features can be obtained upon printing, and that narrow line widths can be obtained.

Multivalent host-guest interactions as described in this chapter, can be used for the development of new nanofabrication schemes. All interactions can be tuned by changing the number and type of guest molecules, which makes the system very versatile, allowing the fabrication of 3D structures[32] as well as structures with interesting electrochemical properties.[4] Furthermore, the controlled attachment of biomolecules at the molecular printboard can be envisioned.

ACKNOWLEDGEMENTS

This work was financially supported by the Council for the Chemical Sciences of The Netherlands Organization for Scientific Research (CW-NWO; M.J.W.L.: Vidi Vernieuwingsimpuls Grant 700.52.423 to J.H.). Dr. Andrea Sartori, Prof. Allesandro Casnati, and Prof. Rocco Ungaro are gratefully acknowledged for the synthesis of calix[4]arenes **4** and **5**.

REFERENCES

1. Beulen, M. W. J., Bügler, J., Lammerink, B., Geurts, F. A. J., Biemond, E. M. E. F., Van Leerdam, K. G. C., Van Veggel, F. C. J. M., Engbersen, J. F. J., Reinhoudt, D. N., *Langmuir* **14**(22), 6424-6429 (1998).
2. Beulen, M. W. J., Bügler, J., De Jong, M. R., Lammerink, B., Huskens, J., Schönherr, H., Vancso, G. J., Boukamp, B. A., Wieder, H., Offenhäuser, A., Knoll, W., Van Veggel, F. C. J. M., Reinhoudt, D. N., *Chem. Eur. J.* **6**(7), 1176-1183 (2000).
3. Huskens, J., Deij, M. A., Reinhoudt, D. N., *Angew. Chem. Int. Ed.* **41**(23), 4467-4471 (2002).
4. Nijhuis, C. A., Huskens, J., Reinhoudt, D. N., *J. Am. Chem. Soc.* **126**(39), 12266-12267 (2004).
5. Rekharsky, M. V., Inoue, Y., *Chem. Rev.* **98**(5), 1875-1917 (1998).
6. Schönherr, H., Beulen, M. W. J., Bügler, J., Huskens, J., Van Veggel, F. C. J. M., Reinhoudt, D. N., Vancso, G. J., *J. Am. Chem. Soc.* **122**(20), 4963-4967 (2000).
7. Auletta, T., Dordi, B., Mulder, A., Sartori, A., Onclin, S., Bruinink, C. M., Péter, M., Nijhuis, C. A., Beijleveld, H., Schönherr, H., Vancso, G. J., Casnati, A., Ungaro, R., Ravoo, B. J., Huskens, J., Reinhoudt, D. N., *Angew. Chem. Int. Ed.* **43**(3), 369-373 (2004).
8. De Jong, M. R., Huskens, J., Reinhoudt, D. N., *Chem. Eur. J.* **7**(19), 4164-4170 (2001).
9. Mammen, M., Choi, S. K., Whitesides, G. M., *Angew. Chem. Int. Ed.* **37**(20), 2754-2794 (1998).
10. Rao, J. H., Lahiri, J., Isaacs, L., Weis, R. M., Whitesides, G. M., *Science* **280**(5364), 708-711 (1998).
11. Rao, J. H., Lahiri, J., Weis, R. M., Whitesides, G. M., *J. Am. Chem. Soc.* **122**(12), 2698-2710 (2000).
12. Gargano, J. M., Ngo, T., Kim, J. Y., Acheson, D. W. K., Lees, W. J., *J. Am. Chem. Soc.* **123**(51), 12909-12910 (2001).
13. Gestwicki, J. E., Cairo, C. W., Strong, L. E., Oetjen, K. A., Kiessling, L. L., J. *Am. Chem. Soc.* **124**(50), 14922-14933 (2002).
14. Gestwicki, J. E., Kiessling, L. L., *Nature* **415**(6867), 81-84 (2002).
15. Huskens, J., Mulder, A., Auletta, T., Nijhuis, C. A., Ludden, M. J. W., Reinhoudt, D. N., *J. Am. Chem. Soc.* **126**(21), 6784-6797 (2004).
16. Mulder, A., Auletta, T., Sartori, A., Del Ciotto, S., Casnati, A., Ungaro, R., Huskens, J., Reinhoudt, D. N., *J. Am. Chem. Soc.* **126**(21), 6627-6636 (2004)
17. Corbellini, F., Mulder, A., Sartori, A., Ludden, M. J. W., Casnati, A., Ungaro, R., Huskens, J., Crego-Calama, M., Reinhoudt, D. N., *J. Am. Chem. Soc.* **126**(51), 17050-17058 (2004).
18. Kitov, P. I., Shimizu, H., Homans, S. W., Bundle, D. R., *J. Am. Chem. Soc.* **125**(11), 3284-3294 (2003).
19. Kramer, R. H., Karpen, J. W., *Nature* **395**(6703), 710-713 (1998).
20. Mandolini, L., *Adv. Phys. Org. Chem.* **22**, 1-111 (1986).
21. Winnik, M. A., *Chem. Rev.* **81**(5), 491-524 (1981).
22. Ercolani, G., *J. Phys. Chem. B* **107**(21), 5052-5057 (2003).
23. Jacobson, H., Stockmayer, W. H., *J. Chem. Phys.* **18**(12), 1600-1606 (1950).
24. Kryschenko, Y. K., Seidel, S. R., Muddiman, D. C., Nepomuceno, A. I., Stang, P. J., *J. Am. Chem. Soc.* **125**(32), 9647-9652 (2003).
25. Warmuth, R., *J. Inclusion Phenom. Macrocyclic Chem.* **37**(1-4), 1-38 (2000).
26. Huisman, B. H., Rudkevich, D. M., Van Veggel, F. C. J. M., Reinhoudt, D. N., *J. Am. Chem. Soc.* **118**(14), 3523-3524 (1996).

27. Huisman, B. H., Rudkevich, D. M., Farrán, A., Verboom, W., Van Veggel, F. C. J. M., Reinhoudt, D. N., *Eur. J. Org. Chem.* **2**, 269-274, (2000).
28. Levi, S. A., Guatteri, P., Van Veggel, F. C. J. M., Vancso, G. J., Dalcanale, E., Reinhoudt, D. N., *Angew. Chem. Int. Ed.* **40**(10), 1892-1896 (2001).
29. Xia, Y., Whitesides, G. M., *Angew. Chem. Int. Ed.* **37**(5), 550-575 (1998).
30. Mirkin, C. A., Hong, S. G., Demers, L., *ChemPhysChem* **2**(1), 37-39 (2001).
31. Piner, R. D., Zhu, J., Xu, F., Hong, S., Mirkin, C. A., *Science* **283**(5402), 661-663 (1999).
32. Crespo-Biel, O., Dordi, B., Reinhoudt, D. N., Huskens, J., *J. Am. Chem. Soc.* **127**(20), 7594-7600 (2005).